

## Rational design of a nonpeptide general chemical scaffold for reversible inhibition of PDZ domain interactions

Naoaki Fujii,<sup>a,†</sup> Jose J. Haresco,<sup>b</sup> Kathleen A. P. Novak,<sup>a</sup> Robert M. Gage,<sup>d</sup> Nicoletta Pedemonte,<sup>c</sup> David Stokoe,<sup>c</sup> Irwin D. Kuntz<sup>a,b</sup> and R. Kiplin Guy<sup>a,d,\*,†</sup>

<sup>a</sup>Department of Pharmaceutical Chemistry, University of California, San Francisco, CA 94143, USA

<sup>b</sup>Laboratory for Molecular Dynamics and Design, University of California, San Francisco, CA 94143, USA

<sup>c</sup>Comprehensive Cancer Center, University of California, San Francisco, CA 94143, USA

<sup>d</sup>Department of Cellular and Molecular Pharmacology, University of California, San Francisco, CA 94143, USA

<sup>e</sup>Laboratory of Molecular Genetics, Giannina Gaslini Institute, Genova 16148, Italy

Received 9 September 2006; revised 2 October 2006; accepted 4 October 2006

Available online 6 October 2006

**Abstract**—Novel small molecules were designed to specifically target the ligand-binding pocket of a PDZ domain. Iterative molecular docking and modeling allowed the design of an indole scaffold **10a** as a reversible inhibitor of ligand binding. The **10a** scaffold inhibited the interaction between MAGI-3 and PTEN and showed cellular activities that are consistent with the inhibition of NHERF-1 function.

© 2006 Elsevier Ltd. All rights reserved.

PDZ domains mediate crucial protein–protein interactions that enforce localization and organization of proteins in a variety of submembranous complexes associated with cell signal mediators, including ion channels, transmembrane receptors, and regulatory enzymes.<sup>1</sup> We have previously reported an irreversible inhibitor of the interaction of a PDZ domain (**1**, Fig. 1).<sup>2</sup> Because drug utility and feasibility are valuable tools for studying cell signaling, their corresponding reversible inhibitors are of great interest. By using small molecules to inhibit PDZ domain interactions, we will be able to evaluate the cellular effect of those interactions by carrying out a cell-based assay. For this purpose, the inhibitors must be cell permeable and able to target PDZ domains whose pharmacological functions are well known such as those of MAGI.

The MAGIs are a subfamily of the MAGUKs, which are widely expressed and have six PDZ domains.<sup>3</sup>

One interaction of MAGI-3 adaptors is between the second PDZ domain (PDZ2) of MAGI and PTEN,<sup>4</sup> a lipid/protein phosphatase. The ITKV motif of the PTEN carboxyl terminus coordinates the interaction of MAGI-3 and PTEN; this interaction suppresses PKB activity by colocalizing PTEN and its substrates. Therefore, chemical disruption of this interaction would be a unique way to investigate its role in coordinating PKB signaling. In this study, we designed a

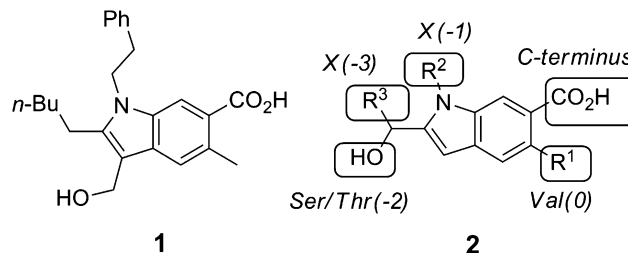


**Figure 1.** Design of novel scaffolds mimicking the side-chain presentation of the four carboxy-terminal residues of the PDZ domain's ligand. (1) Irreversible inhibitor based on spontaneous ionization of a 3-hydroxymethyl indole. (2) Designed scaffold and targeted variations. **R**<sup>1</sup> indicates variable replacement for the (0) ligand residue side-chain; **R**<sup>2</sup> indicates variable replacement for the (–1) ligand residue side-chain; and **R**<sup>3</sup> indicates variable replacement for the (–3) ligand residue side-chain.

**Keywords:** PDZ domain; Protein–protein; Interaction; Drug design; NHERF.

\* Corresponding author. Tel.: +1 901 495 5714; fax: +1 901 495 5715; e-mail: Kip.Guy@stjude.org

† Present address: Department of Chemical Biology and Therapeutics, MS 1000, St. Jude Children's Research Hospital, 332 N. Lauderdale, Memphis, TN 38105-2794, USA.

general chemical scaffold for PDZ-domain-binding based on a canonical PDZ-domain structure and then tailored the scaffold to mimic I-T/S-X-V to investigate on MAGI-3.

Analysis of the structure of PSD-95 PDZ3 bound with KQTSV ligand<sup>5</sup> revealed the geometry of the ligand. Inspection of the  $\beta$ -strand ligand revealed that its conformation was uncharacteristic of other  $\beta$  strands. The typical  $\phi/\psi$  angles of an antiparallel  $\beta$  strand are  $113^\circ/180^\circ$ . For the PDZ domain, these angles are  $117.7^\circ/110.4^\circ$ ,  $-106.6^\circ/149.3^\circ$ , and  $-101.9^\circ/178.4^\circ$ , for the 0,  $-1$ , and  $-2$  residues, respectively.

This uncharacteristic conformation allows the side-chain of Val(0) to dip toward the hydrophobic cavity in the PDZ-domain-binding groove. To preserve the orientations of the carboxylate and the Val(0) side-chain, we measured the distances and angles between the  $\alpha$  carbons of residues 0 and  $-1$  by using Weblab (Accelrys, San Diego, CA) and then manually matched them to those of simple heterocyclic rigid cores. Among the evaluated heterocycles, only indole or benzothiophene adequately preserved the requisite distance and angle restraints and accommodated all positions for functions deemed necessary for the matching. On the basis of the indole's presence in a number of drugs and feasibility in chemical modification for chemical library approach, we focused on it. Scaffold **2** (Fig. 1) included positions R<sup>1</sup> through R<sup>3</sup> that projected various functions to optimize the mimicry of peptide ligand side-chains into the PDZ-domain-binding pocket. Initial docking experiments with the indole scaffold **2** indicated that it could indeed place critical functional groups in proximity to the orientation of the  $\beta$ -strand conformation of bound ligand in the crystal structure (Fig. 2). The R<sup>2</sup> position of the indole scaffold **2** has an optimal orientation for presenting the group to mimic the  $-1$  side-chain or other functional groups. However, PSD-95 PDZ3, whose structure was used for these docking experiments, does not make tight contacts with the Ser ( $-1$ ) side-chain in the KQTSV ligand. Our analysis of this structure indicated similarly that the hydroxyalkyl groups evaluated at the R<sup>2</sup> position did not make contacts with the PDZ domain, nor did they appear to substantially contribute to the overall scores. Introducing a hydroxyalkyl group at the R<sup>2</sup> position made the molecule too hydrophilic; therefore, it would not be cell permeable. Thus, a simple 2-phenylethyl group was chosen as the R<sup>2</sup> group to add the proper hydrophobicity to make the molecule cell permeable. The *n*-butyl group in **10a** was considered a suitable alternative for the M/I( $-3$ ) alkyl side-chain of the M/I-TXV peptide. Compound **10a** can successfully make all of the following necessary contacts to mimic the  $\beta$  strand: (1) a carboxylic acid mimics the C-terminus of the peptide ligand; (2) a methyl group at the R<sup>1</sup> position fills the hydrophobic pocket that the Val(0) side-chain normally occupies; and (3) a nonpeptide extension at the R<sup>3</sup> position places a hydroxy group within hydrogen bonding distance to histidine residue (Fig. 2D). This potential is supported by DOCKs energy scoring:  $-26.31$  for **10a** (Fig. 2C) versus  $-20.00$  for the KQTSV  $\beta$  strand (Fig. 2A).

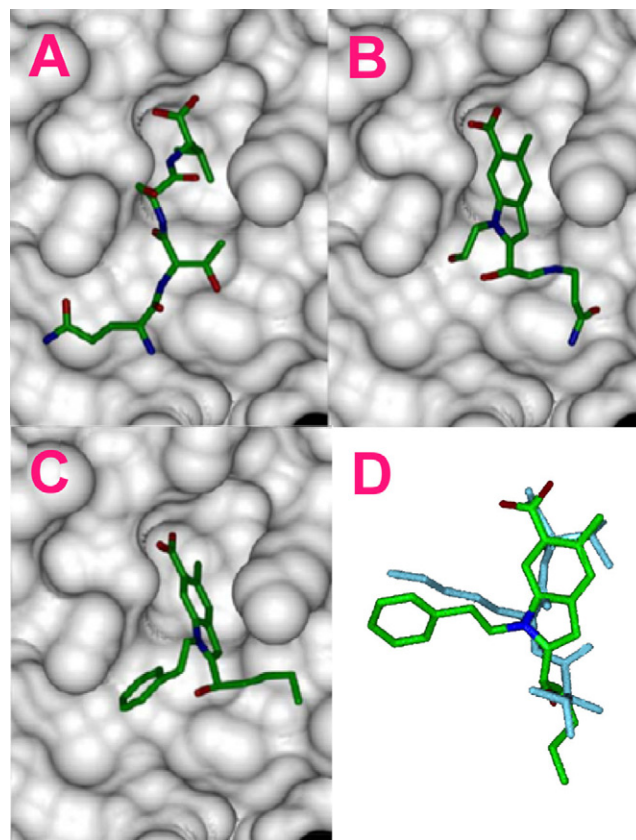


**Figure 2.** Optimization of scaffold design by virtual library screening. (A) KQTSV peptide (DOCK score:  $-20$ ). (B) The results of substitution of position R<sup>1</sup> on an initially designed scaffold (DOCK score:  $-30$ ). (C) Designed reversible inhibitor **10a** (DOCK score:  $-27$ ). (D) The overlay of targeted reversible inhibitor **10a** (green) with the native ligand, KQTSV peptide (blue).

We envisioned a synthetic route to **10a** allowing full variation of the highlighted variable groups by a library approach (Fig. 3). The carboxyl group of 2-methyl-5-nitrobenzoic acid **3** was protected, and the nitro group was then reduced to give aniline **4**. Iodination of **4** with iodine monochloride gave a mixture of **5a** and **5b**. The undesired product **5b** was easily separated by chromatography and recycled to **4**. Iodoaniline **5a** was coupled with ethyl pyruvate in the presence of palladium acetate<sup>6</sup> to give indole **6**, which was easily converted to aldehyde **7**. The aldehyde **7** is the foundation for developing the library that has diverse substituents on its indole-1 (R<sup>2</sup>) and indole-2 (R<sup>3</sup>) positions by sequential electrophilic and nucleophilic alkylation. The 2-phenylethyl group was attached to the indole-1 position of **7**, and the *n*-butyl group was attached to the indole-2 position and deprotected to give I-TXV mimetic **10a**. Sodium salt of **10a** has good solubility ( $>30$  mM) in water that does not contain DMSO.

We have shown that pre-incubation with irreversible inhibitor **1** blocks peptide-ligand binding and that **1** forms a stoichiometric irreversible adduct with the MAGI-3 PDZ2 domain.<sup>2</sup> In contrast, **10a** did not affect the pre-incubation. Longer incubation of the PDZ with **1** increased the inhibitory efficacy in a time-dependent

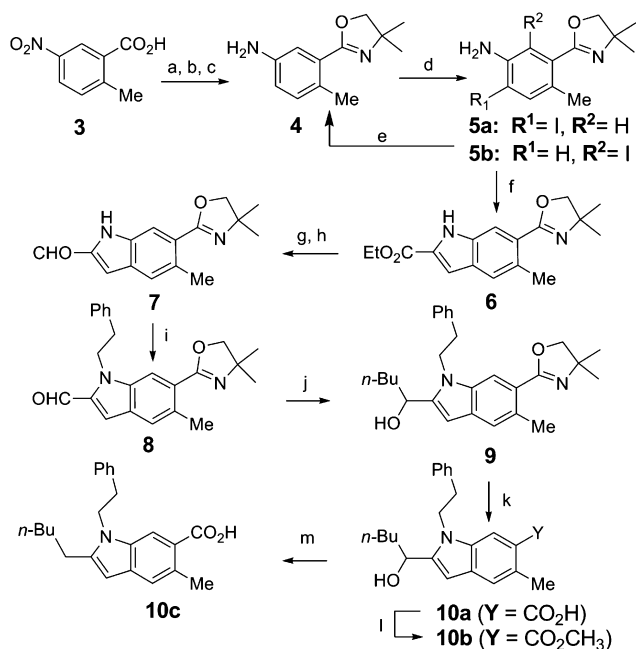


**Figure 3.** Synthesis of **10a–c**. (a) HOCH<sub>2</sub>C(CH<sub>3</sub>)<sub>2</sub>NH<sub>2</sub> (3 equiv), HBTU (1.2 equiv), DIPEA (2 equiv), DMF, 40 °C, 14 h; (b) SOCl<sub>2</sub> (5 equiv), CH<sub>2</sub>Cl<sub>2</sub>, rt, 0.5 h; (c) Fe (7.8 equiv), NH<sub>4</sub>Cl (aq), EtOH, reflux, 3 h, 92% over 3 steps; (d) ICl (1.6 equiv), CaCO<sub>3</sub> (3 equiv), MeOH, H<sub>2</sub>O, rt, 1 h. **5a**: 36%, **5b**: 47%; (e) H<sub>2</sub>, Pd–C, MeOH, Et<sub>3</sub>N, rt, 1 h, quant; (f) ethyl pyruvate (5 equiv), Pd(OAc)<sub>2</sub> (0.2 equiv), DABCO (5 equiv), DMF, 105 °C, 50 min, 44%; (g) LiAlH<sub>4</sub> (10 mol equiv), THF, reflux, 2.5 h, 75%; (h) MnO<sub>2</sub> (1.8 equiv), CH<sub>2</sub>Cl<sub>2</sub>, rt, 12 h, 76%; (i) BrCH<sub>2</sub>CH<sub>2</sub>Ph (5 equiv), K<sub>2</sub>CO<sub>3</sub> (10 equiv), DMF, 40 °C, 22 h, 93%; (j) *n*-BuMgBr (5 equiv), 0 °C, 0.5 h, 87%; (k) *i*-MeI (large excess), K<sub>2</sub>CO<sub>3</sub> (3 equiv), acetone, rt, 2.5 d; ii—NaOH, H<sub>2</sub>O, MeOH, reflux, 7 h, 2 steps overall 89%; (l) MeI (large excess), K<sub>2</sub>CO<sub>3</sub> (large excess), acetone, rt, 1.5 h, 69%; (m) H<sub>2</sub>, 10% Pd–C, HCl (20 equiv), MeOH, rt, 1 h, 25%.

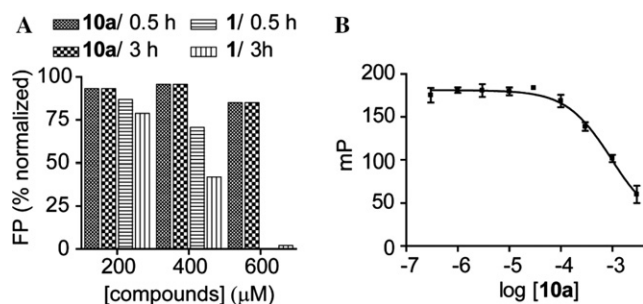


**Figure 4.** (A) Comparison of the effects of reversible inhibitor **10a** and irreversible inhibitor **1**. The protein and inhibitors were allowed to equilibrate for the indicated times at 4 °C and were incubated with the OregonGreen-PFDEDQHTQITV peptide ligand for 0.5 h to measure the fluorescent polarization (FP). Data are reported as % normalized by control experiments (no compounds). (B) Titration curve for competitive inhibition of PDZ domain–ligand binding, as measured by fluorescence polarization. The fluorescent peptide probe and protein were allowed to equilibrate for 0.5 h with increasing concentrations of **10a**; mP = milipolarization units.

manner, whereas **10a** did not (Fig. 4A). Therefore, the inhibitory effect of **10a** is reversible. To investigate if **10a** non-specifically targets other proteins in cells, we have prepared biotin-tagged **10a** to treat with crude

lysates of several cancer cell lines. No biotinylated bands were observed in Western analysis (streptavidin blotting) of the biotin-**10a** treated lysate sample, whereas biotin-**1** visualized many protein bands under the identical conditions (data not shown). This result suggests that **10a** does not covalently modify any proteins, while **1** does.

If **10a** binds to PDZ domains as an ITXV mimic, chemical modifications analogous to mutations that block ligand binding should destroy its binding activity. Variations of **10a** with altered substituents correspond to altered carboxyl terminus and Thr(–2) hydroxyl group, respectively, in ITXV peptide. From this viewpoint, **10b** and **10c** were designed as mimetics of those inactive mutant peptides. Compound **10a** had affinity for the MAGI-3 PDZ2 domain, as demonstrated by its ability to displace a peptide probe by fluorescent polarization method,<sup>7</sup> in a concentration-dependent manner (Fig. 4B). The competition was observed with concentrations of **10a** in the range of >100 μM. AlphaScreen energy transfer assay<sup>8</sup> also afforded a similar competition curve (data not shown). Meanwhile, negative controls **10b** and **10c**, in which moieties required for the PDZ ligand interaction were disrupted, did not show any competition (data not shown). The **10a** scaffold (50 μM) doubled the level of PKB kinase activity in the HCT116 cell line that expresses wild-type PTEN; this finding suggests that co-localization of PTEN is inhibited in cells. This activity level is reasonable in comparison with **1**, which inhibited the MAGI-3/PTEN interaction more potently (~50% reduction of binding response at 10 μM) and activated PKB (~3 times at 5 μM).<sup>2</sup>

An important feature of the chemistry presented (Fig. 3) is its feasibility to make diverse libraries highly variant in the R<sup>2</sup> and R<sup>3</sup> positions to discover class- and domain-selective inhibitors. Therefore, the scaffold described herein offers several opportunities for optimization toward other specific PDZ domains. To investigate whether **10a** can serve as a basis of such optimization for targeting other PDZ domains, we have focused on the first PDZ domain (PDZ1) of NHERF-1.<sup>9</sup> The NHERF-1 PDZ1 binds to the D-T/S-X-L motif of the β<sub>2</sub>-adrenergic receptor to recycle it from the endocytosed fraction at the cell surface<sup>10</sup> and cystic fibrosis transmembrane conductance regulator (CFTR) to control channel gating.<sup>11</sup> We treated HEK293 cells with **10a**; these cells stably expressed tagged β<sub>2</sub>-adrenergic receptor or a delta δ-opioid receptor chimera that had a carboxyl-terminus sequence of β<sub>1</sub>-adrenergic receptor that is not recycled back by NHERF-1.<sup>10</sup> The expression level of these receptors on the cellular surface was quantified. Only the expression of the β<sub>2</sub>-adrenergic receptor was reduced in a dose-dependent manner, suggesting inhibition of recycling (Fig. 5A). The **10a** inhibitor was then tested in short-circuit current experiments on human bronchial epithelial cells in which the basolateral membrane had been permeabilized. The **10a** inhibited CFTR-mediated chloride transport in a weak but dose-dependent manner (Fig. 5B). Together, these results suggest that **10a** weakly inhibits interaction at the NHERF-1 PDZ1 domain. Structural analysis revealed the importance of hydrogen

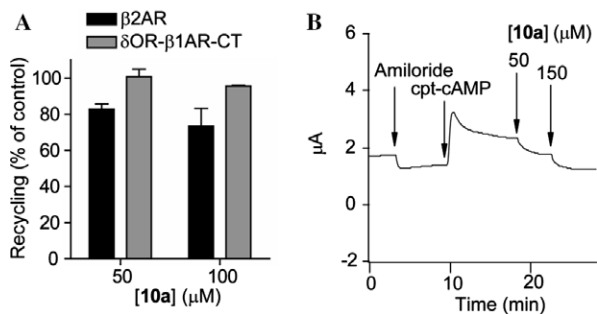


**Figure 5.** (A) Inhibition of receptor recycling in HEK-293 cells. Receptors were stimulated by each agonist; the receptor tags were labeled with antibodies (FLAG); and surface receptors were quantified by flow cytometry. The **10a** inhibitor was added 0.5 h prior to the internalization step. The indicated concentration of **10a** was carried through all subsequent steps. (B) Short-circuit current in permeabilized human bronchial epithelial cells expressing human CFTR. CFTR expression was stimulated by 100 μM CPT-cAMP, and **10a** was added in the apical bathing solution. The current was continuously recorded using a voltage clamp.

bond interaction on the D(–3) of the PDZ1 ligand.<sup>12</sup> On the basis of that study, the design and evaluation of another compound with an R<sup>3</sup> substitution mimicking the D(–3) side-chain are underway.

We have found another indole-2-carbinol scaffold compound showing >10 times potency in antagonizing the interaction of Dishevelled (DVL) PDZ domain than that of MAGI-3 PDZ2 (unpublished data). This shows high potential of **10a** as seed scaffold for further optimization. This study will be reported in due course.

#### Acknowledgments

We thank Angela McArthur for scientific editing of the manuscript. Financial support was provided in part by

the Fujisawa Pharmaceutical Co., Ltd. (NF), the UCSF Stuart Trust Fund (NF, KAN, RKG), the Sandler Research Foundation, and the Sidney Kimmel Research Foundation (NF, RKG).

#### Supplementary data

Synthetic procedure, analysis data, and protocols for biochemical assay and cell-based assay. Supplementary data associated with this article can be found, in the on-line version, at doi:10.1016/j.bmcl.2006.10.006.

#### References and notes

- Harris, B. Z.; Lim, W. A. *J. Cell Sci.* **2001**, *114*, 3219.
- Fujii, N.; Haresco, J. J.; Novak, K. A.; Stokoe, D.; Kuntz, I. D.; Guy, R. K. *J. Am. Chem. Soc.* **2003**, *125*, 12074.
- Dobrosotskaya, I.; Guy, R. K.; James, G. L. *J. Biol. Chem.* **1997**, *272*, 31589.
- Wu, Y.; Dowbenko, D.; Spencer, S.; Laura, R.; Lee, J.; Gu, Q.; Lasky, L. A. *J. Biol. Chem.* **2000**, *275*, 21477.
- Doyle, D. A.; Lee, A.; Lewis, J.; Kim, E.; Sheng, M.; MacKinnon, R. *Cell* **1996**, *85*, 1067.
- Chen Cy, C.; Lieberman, D. R.; Larsen, R. D.; Verhoeven, T. R.; Reider, P. J. *J. Org. Chem.* **1997**, *62*, 2676.
- Novak, K. A.; Fujii, N.; Guy, R. K. *Bioorg. Med. Chem. Lett.* **2002**, *12*, 2471.
- Wilson, J.; Rossi, C. P.; Carboni, S.; Fremaux, C.; Perrin, D.; Soto, C.; Kosco-Vilbois, M.; Scheer, A. *J. Biomol. Screen.* **2003**, *8*, 522.
- Hall, R. A.; Ostedgaard, L. S.; Premont, R. T.; Blitzer, J. T.; Rahman, N.; Welsh, M. J.; Lefkowitz, R. J. *Proc. Natl. Acad. Sci. U.S.A.* **1998**, *95*, 8496.
- Gage, R. M.; Matveeva, E. A.; Whiteheart, S. W.; von Zastrow, M. *J. Biol. Chem.* **2005**, *280*, 3305.
- Raghuram, V.; Mak, D. D.; Foskett, J. K. *Proc. Natl. Acad. Sci. U.S.A.* **2001**, *98*, 1300.
- Karthikeyan, S.; Leung, T.; Ladias, J. A. *J. Biol. Chem.* **2001**, *276*, 19683.